ISSN 1063-7761, Journal of Experimental and Theoretical Physics, 2007, Vol. 104, No. 5, pp. 766–774. © Pleiades Publishing, Inc., 2007.
Original Russian Text © S.S. Aplesnin, 2007, published in Zhurnal Éksperimental'noĭ i Teoreticheskoĭ Fiziki, 2007, Vol. 131, No. 5, pp. 878–887.

ORDER, DISORDER, AND PHASE TRANSITION IN CONDENSED SYSTEMS

Effect of Bond Fluctuations on the Transport Properties of Manganites and Nickelates

S. S. Aplesnin

Kirensky Institute of Physics, Siberian Division, Russian Academy of Sciences, Akademgorodok, Krasnoyarsk, 660036 Russia
Reshetnev Siberian State Aerospace University, Krasnoyarsk, 660014 Russia
e-mail: apl@iph.krasn.ru

Received October 23, 2006

Abstract—For the manganites $RMnO_3$ (R = La, Pr, Nd), a mechanism is proposed to explain the anomalous temperature dependences of the kinetic coefficients, resistivity, and thermoelectric power during the transition from the pseudocubic *O* to the orthorhombic *O*' crystal structure. The contributions of the bending and stretching modes of the octahedron to the formation of thermal-conductivity maxima and to the deviation from the linear dependence of $\ln(\rho/T)$ on $1/T$ at low temperatures have been estimated. In nickelates, the metal–insulator transition is caused by lattice-polaron pinning by the stretching mode of the octahedron, and the low-temperature anomaly of the thermal conductivity is related to electron scattering by the bending mode of the octahedron.

PACS numbers: 72.20.-i, 72.20.Nz, 72.15.Qm

DOI: 10.1134/S1063776107050111

1. INTRODUCTION

Charge ordering often occurs in the oxides of transition metals, and it is of particular interest due to the presence of a giant magnetoresistance in manganites and of a metal–insulator (MI) transition in $ANiO_3$ (A = Y, Pr, Nd, …) [1]. The charge disproportionation $Me^{+3} = Me^{+3-\delta} + Me^{+3+\delta}$ is common for the perovskites $AMeO_3$ (A = Pr, Nd, …, Me = Mn, Co, Ni) and is closely related to a sharp increase in the conductivity below a certain critical temperature. For example, the change in the resistivity ρ is maximum in a temperature range $T^* < T < T_{JT}$, where T^* is the orbital disordering temperature and T_{JT} is the ordering temperature for the Jahn–Teller cooperative distortions of the octahedron [2]. The $AMnO_3$ (A = La, Pr, Nd, …) family exhibits a gap in a one-particle electron excitation spectrum, and the resistivity is described by a polaron-type equation $\rho(T) = AT\exp(-E_a/T)$ in a narrow temperature range [2]. Both at $T > T_{JT}$ and $T < T^*$, the conductivity has a semiconductor character with an activation energy $0.3 < E_a < 1.2$ eV, and the activation energy for lanthanum is unchanged in the temperature range $T > T_{JT}$ and $T < T^*$. The spectral weight of the optical conductivity changes toward low energies upon heating above the temperature T_{JT} [3]. Neutron data obtained for a high-resolution atomic pair distribution function indicate local octahedron distortions that are retained in clusters ~16 Å ~ $4MnO_6$ in diameter [4] without changes in the angle of octahedron inclination in a cluster. The authors of [2] explained the resistance anomaly at $T < T_{JT}$ by the charge disproportionation of Mn^{3+} ions on Mn^{2+} and Mn^{4+}. However, the total disproportionation reaction gives a spin $\mu_{eff} = 5.0\mu_B$, which differs from the experimental data for localized Mn^{3+} at a temperature $T > T_{JT}$ ($\mu = 5.22\mu_B$) and at a temperature $T < T^*$ ($\mu = 4.89\mu_B$) [5]. The temperature independence of the thermopower coefficient at $T > T_{JT}$ and a high Debye–Waller factor [6] in the vicinity of $T \sim T_{JT}$ indicate a heavy effective carrier mass.

The Ni^{3+} ion has an electronic configuration e_g that is analogous to that of Mn^{3+} with strong *p–d* hybridization. The electronic state of the Ni^{3+} ion in the octahedron is close to $Ni^{2+}\underline{L}$ (a hole in the ligand on the oxygen ion of the 2*p* orbital) [7], and the charge disproportionation can be represented as $2Ni^{2+}\underline{L} \longrightarrow Ni^{2+} + Ni^{2+}\underline{L}^{2\delta}$, where holes on oxygen play a key role. Structural and magnetic studies indicate the presence of large inhomogeneous regions in both the metallic and dielectric phases. X-ray spectroscopy performed with a Ni*K* line detected different Ni–O bond lengths within the first coordination shell: $\Delta\sigma^2_{Ni-O} \approx 0.0012$ Å^2 [8]. In the MI transition range, the $ANiO_3$ family exhibits a smooth decrease in the spectral density in the energy range $\Delta E = E - E_F \sim 0.6$ eV for A = Pr, Nd ions and no changes in $g(E_F)$ for A = Sm, Eu [9]. The temperature evolution of the spectral density at the Fermi level and the temperature behavior of the resistivity differ substantially. For example, compounds with $T_N = T_{MI}$ exhibit a temperature hysteresis in $\rho(T)$. Correlation effects with the participation of mixed d^7, $d^8\underline{L}$, and $d^9\underline{L}^2$ states decrease the covalent effects with decreasing temperature and change the electronic structure over a

wide temperature range. The $\rho(T)$ is more adequately described with a charge-ordering model related to the ordering of the Ni–O bonds, which correlates with a giant isotopic effect at T_{MI}. This effect demonstrates oxygen-atom displacement fluctuations, which, in turn, modulate the Ni–O bond length [10].

The $ATiO_3$ family with the electron configuration d^1 does not exhibit an MI transition in compounds with metallic conduction ($LaTiO_3$). Nevertheless, orbital ordering with an orthorhombic lattice distortion below the Néel temperature ($T_N = 146$ K) is also realized here [11], and the Mott–Hubbard dielectric $YTiO_3$ with a gap in the electron excitation spectrum ($\Delta \approx 0.8$ eV) has a typical semiconductor character [12]. The oxides of Ti and V have a perovskite-like structure and do not exhibit charge disproportionation and Ti–O and V–O bond fluctuations. An analysis of the experimental data indicates that charge ordering and metal–oxygen bond length fluctuations are possible in the $AMeO_3$ compounds, where the electron configuration of the metal is e_g. The formation of the covalent bond d_{3z^2}–p_z (hereafter, the orbital $d_{3z^2-r^2}$ is designated as d_{3z^2}) would change the M–O bond length between neighboring cation ions, which are retained above the temperature T_{JT}, T_{MI} (e.g., in $LaMnO_3$, at $T = 840$ K, $d(\text{Mn–O}_{\text{short}}) = 1.92$ Å and $d(\text{Mn–O}_{\text{long}}) = 2.13$ Å remain virtually unchanged at $T > T_{JT}$, T_{MI} [13]); that is, bonds are ordered below the critical temperature. The electron density on the cation increases due to bond polarity, and, according to x-ray diffraction data, the weights of the $3d^5\underline{L}^1$ and $3d^6\underline{L}^2$ states are approximately 41 and 9% [14], which corresponds to one- and two-hole states on oxygen ions, respectively. A hole on the oxygen ligand $O^{2-\delta}$ is attracted to a positive rare-earth ion and changes the M–O–M bond angle, whose value increases with the ordinal number of the rare-earth element in the periodic table. For example, $\theta = 155°$ (La), 152° (Pr), 149° (Nd), and 147° (Sm) in $RMnO_3$ [2] and $\theta = 165.2°$ (La), 158.7° (Pr), 152.6° (Sm), and 151.7° (Ho) in $RNiO_3$ [15]. The local structural distortions induce hybridization of the $p_{x,y}$ oxygen orbitals with d_{3z^2}. As a result, an electron can pass between neighboring metal ions through an oxygen ion, which is accompanied by electron exchange between oxygen orbitals.

2. MODEL AND CALCULATION PROCEDURE

Charge ordering is assumed to be represented by a certain order of the covalent bonds $3d_{3\alpha^2} - 2p_\alpha$ and $3d_{3\alpha^2} - 2p_{\beta,\gamma}$ ($\alpha, \beta, \gamma = x, y, z$); that is, the metal cation Mn^{3+} or Ni^{3+} can contain two strong bonds with an overlap integral $V_{p_z, 3z^2} \approx 2$ eV [16], two weak bonds with $V_{p_{x,y}, 3z^2} \ll 2$ eV, or one $M^{+3-\delta}$–O–$M^{+3} \Rightarrow M^{+3}$–O–$M^{+3-\delta}$ bond. In the latter case, the center of symmetry for the metal–oxygen–metal hopping integral is absent, which is characteristic of manganites. The strong $V_{p_\alpha, 3\alpha^2}$ bonds favor the contraction of the octahedron along a bond direction, and the weak $V_{p_{\beta,\gamma}, 3\alpha^2}$ bonds rotate the octahedron, which can be related to the corresponding vibration modes $\omega_{\text{stretching}} \sim 550$ cm^{-1} (La) and 607 cm^{-1} (Nd) and $\omega_{\text{bending}} \sim 350$ (La) [17] and 450 cm^{-1} (Nd) [18] in $RMnO_3$. These compounds have p-type conduction, and the transfer of an electron density between the p_α oxygen orbitals depends on the splitting of the energy levels of these orbitals induced by the crystal field created by rare-earth ions.

Thus, in our model, charge transfer occurs via one-electron hopping along oxygen sites, and the electronic states on the $3d_{z^2}$ metal ions are localized on the assumption that the Fermi level lies between binding and antibinding orbitals. The thermoelectric power and thermal conductivity are contributed by both one-particle and two-particle (electron + hole) electron excitations, which simulate the transfer of the covalent bond. In turn, this bond can be described by two-electron excitations in a crystal lattice and be represented in the form $M^{+3-\delta}$–O–$M^{+3} \Rightarrow M^{+3}$–O–$M^{+3-\delta}$. The effective charge transfer Hamiltonian is

$$
\begin{aligned}
H &= H_0 + H_1 + H_2,\\
H_0 &= \sum_i (\epsilon_d - \mu) c_i^+ c_i + \sum_{\alpha,i} (\mu - \epsilon_o) a_{\alpha,i}^+ a_{\alpha,i}\\
&\quad - \sum_{i,j} t_{1,ij} (a_{1,i}^+ a_{2,j} + a_{1,i} a_{2,j}^+)\\
&\quad - \sum_{i,k,\alpha,\beta} t_{2,i,k} (c_i^+ a_{\alpha,i} a_{\beta,k}^+ c_k + c_i a_{\alpha,i}^+ a_{\beta,k} c_k^+)\\
&\quad + \sum_{i,\alpha,\beta} \Delta_i (a_{1,i}^+ a_{1,i} - a_{2,i}^+ a_{2,i})\\
&\quad + \sum_{\alpha,i,j} U n_{a1,i} n_{a2,j},\\
H_1 &= \sum_{i,k,q} g_{1,iq} (a_{1,i} c_i^+ + a_{1,i}^+ c_i)(b_{-q}^+ + b_q)\\
&\quad + g_{2,kq} (a_{2,k} c_k^+ + a_{2,k}^+ c_k)(p_{-q}^+ + p_q),\\
H_2 &= \sum_{\mathbf{q}} (\omega_{1q} b_q^+ b_q + \omega_{2q} p_q^+ p_q).
\end{aligned}
\tag{1}
$$

Here, $\epsilon_{d,o}$ are the electronic levels in $3d$-metal atoms and oxygen ions, respectively; t_1 is the electron hopping integral for the p_x and p_y orbitals; the third term

describes the transfer of the covalent bond $V_{p_\beta, 3\alpha^2}$ ($\alpha, \beta = x, y, z$) in the simple cubic lattice; summation is taken over M–O bonds; c^+ and a are the operators of electron creation and annihilation by metal and oxygen ions, respectively; Δ is the parameter of the crystal splitting of the orbital triplet by an oxygen ion, which is determined by the multipole interaction of oxygen ions with rare-earth ions; and g_1 and g_2 are the interaction parameters of the electron density on the M–O bond with the bending (ω_1) and stretching (ω_2) modes of the octahedron, respectively.

We set up a set of equations for electrons and holes by making allowance for retained second-order operators. In the random-phase approximation, these equations have the form

$$
\begin{aligned}
i\frac{d}{dt}a_{1,i} &= -(\epsilon_o - \mu - \Delta - Un_{a2})a_{1,i} \\
&- \sum_h t_{1i,i+h}a_{2,i+h} + \sum_q g_{1,iq}c_i(b_q^+ + b_{-q}), \\
i\frac{d}{dt}a_{2,i} &= -(\epsilon_o - \mu + \Delta - Un_{a1})a_{2,i} \\
&+ \sum_h t_{1i,i+h}a_{1,i+h} + \sum_q g_{2,iq}c_i(p_q^+ + p_{-q}), \\
i\frac{d}{dt}c_i &= -(\epsilon_d + \mu)c_i - \sum_q g_{1,iq}a_{1,i}(b_q^+ + b_{-q}) \\
&- \sum_q g_{2,iq}a_{2,i}(p_q^+ + p_{-q}), \\
i\frac{d}{dt}(a_{1,i}b_{-q}) &= -(\epsilon_o - \mu - \Delta - Un_{a2} - \omega_{1,-q}n_{-q}) \\
&\times (a_{1,i}b_{-q}) - g_{1,iq}(1 + n_{-q} - n_{a1})c_i, \\
i\frac{d}{dt}(a_{1,i}b_q^+) &= -(\epsilon_o - \mu - \Delta - Un_{a2} + \omega_{1,q}n_q) \\
&\times (a_{1,i}b_q^+) + g_{1,iq}(n_q + n_{a1})c_i, \\
i\frac{d}{dt}(a_{2,i}p_{-q}) &= -(\epsilon_o - \mu + \Delta - Un_{a1} - \omega_{2,-q}n_{-p}) \\
&\times (a_{2,i}p_{-q}) - g_{2,iq}(1 + n_{-q} - n_{a2})c_i, \\
i\frac{d}{dt}(a_{2,i}p_q^+) &= -(\epsilon_o - \mu + \Delta - Un_{a1} + \omega_{2,q}n_p) \\
&\times (a_{2,i}p_q^+) + g_{2,iq}(n_p + n_{a2})c_i, \\
i\frac{d}{dt}(c_ib_{-q}) &= (\epsilon_d - \mu + n_{-q}\omega_{1,-q})(c_ib_{-q}) \\
&- g_{1,iq}(1 + n_{-q} - n_c)a_{1,i}, \\
i\frac{d}{dt}(c_ib_q^+) &= (\epsilon_d - \mu + n_q\omega_{1,q}) \\
&\times (c_ib_q^+) - g_{1,iq}(n_q + n_c)a_{1,i}, \\
i\frac{d}{dt}(c_ip_q^+) &= (\epsilon_d - \mu - n_p\omega_{2q}) \\
&\times (c_ip_q^+) - g_{2,iq}(n_p + n_c)a_{2,i}, \\
i\frac{d}{dt}(c_ip_{-q}) &= (\epsilon_d - \mu + n_{-p}\omega_{2,q}) \\
&\times (c_ip_{-q}) - g_{2,iq}(1 + n_{-p} - n_c)a_{2,i},
\end{aligned}
\tag{2}
$$

where n_{-q}, n_q, n_{-p}, and n_p are the mean phonon occupation numbers due to the symmetry of optical phonon modes with respect to the center of the band, $n_{-q} = n_q$ and $n_{-p} = n_p$. These numbers are defined as $n_{q,p} = (\exp(h\omega_{1,2}/kT) - 1)^{-1}$. The band occupation parameters n_c and $n_{a1,2}$ specify the position of the chemical potential.

Green's functions for holes ($G_{\mathbf{k}}^{\alpha\alpha} = \langle\langle a_{\alpha,\mathbf{k}}|a_{\alpha,\mathbf{k}}^+\rangle\rangle$) and polarons ($G_{\mathbf{k}+\mathbf{q}}^{cb^+\alpha} = \langle\langle c_{\mathbf{k}}b_{\mathbf{k}+\mathbf{q}}^+|a_{\alpha,\mathbf{k}}^+\rangle\rangle$ and $G_{\mathbf{k}-\mathbf{q}}^{cp\alpha} = \langle\langle c_{\mathbf{k}}p_{\mathbf{k}-\mathbf{q}}|a_{\alpha,\mathbf{k}}^+\rangle\rangle$) have the form

$$
\begin{aligned}
&(\omega + a_{\alpha\alpha})G_{\mathbf{k}}^{\alpha\beta} + \epsilon_1(\mathbf{k})G_{\mathbf{k}}^{\beta\beta} \\
&- g_{\alpha\mathbf{kq}}(G_{\mathbf{k}+\mathbf{q}}^{cb^+\alpha} + G_{\mathbf{k}-\mathbf{q}}^{cb\alpha}) = 0, \\
&-\epsilon_1(\mathbf{k})G_{\mathbf{k}}^{\alpha\beta} + (\omega + a_{\beta\beta})G_{\mathbf{k}}^{\beta\beta} \\
&- g_{\beta\mathbf{kq}}(G_{\mathbf{k}+\mathbf{q}}^{cb^+\beta} + G_{\mathbf{k}-\mathbf{q}}^{cb\beta}) = 1, \\
&g_{\alpha\mathbf{kq}}(n_q + n_c)G_{\mathbf{k}}^{\alpha\beta} \\
&+ G_{\mathbf{k}+\mathbf{q}}^{cb^+\beta}(\omega + \epsilon_d + \mu + n_q\omega_{\alpha,q}) = 0, \\
&g_{\alpha\mathbf{kq}}(1 + n_q - n_c)G_{\mathbf{k}}^{\alpha\beta} \\
&+ G_{\mathbf{k}-\mathbf{q}}^{cb\beta}(\omega + \epsilon_d + \mu - n_q\omega_{\alpha,q}) = 0, \\
&g_{\beta\mathbf{kq}}(n_p + n_c)G_{\mathbf{k}}^{\beta\beta} \\
&+ G_{\mathbf{k}+\mathbf{q}}^{cp^+\beta}(\omega + \epsilon_d + \mu + n_p\omega_{\beta,q}) = 0, \\
&g_{\beta\mathbf{kq}}(1 + n_p - n_c)G_{\mathbf{k}}^{\beta\beta} \\
&+ G_{\mathbf{k}-\mathbf{q}}^{cp\beta}(\omega + \epsilon_d + \mu - n_p\omega_{\beta,q}) = 0, \\
&\epsilon_1(\mathbf{k}) = -2t_1\left(\cos\left(\frac{k_x}{2}\right)\cos\left(\frac{k_y}{2}\right)\right. \\
&\left.+ \lambda\left(\cos\left(\frac{k_z}{2}\right)\cos\left(\frac{k_x}{2}\right) + \cos\left(\frac{k_z}{2}\right)\cos\left(\frac{k_y}{2}\right)\right)\right),
\end{aligned}
\tag{3}
$$

where the parameter λ describes the anisotropy of the hopping integrals in a plane and between planes. Hereafter, we use $\lambda = 0.25$. Green's functions for electrons ($G^{cc}_{\mathbf{k}} = \langle\langle c_{\mathbf{k}}|c^+_{\mathbf{k}}\rangle\rangle$) and polarons ($G^{ab^+}_{\mathbf{k+q}} = \langle\langle a_{\alpha,\mathbf{k}} b^+_{\mathbf{k+q}}|c^+_{\mathbf{k}}\rangle\rangle$ and $G^{\alpha p}_{\mathbf{k-q}} = \langle\langle a_{\alpha,\mathbf{k}} p_{\mathbf{k-q}}|c^+_{\mathbf{k}}\rangle\rangle$) make up the set of equations

$$\begin{gathered}
(\omega+\epsilon_d+\mu)G^{cc}_{\mathbf{k}} + g_{1\mathbf{kq}}(G^{1b^+}_{\mathbf{k+q}} + G^{1b}_{\mathbf{k-q}}) \\
+ g_{2\mathbf{kq}}(G^{2p^+}_{\mathbf{k+q}} + G^{2p}_{\mathbf{k-q}}) = 1, \\
-g_{1\mathbf{kq}}(n_q + n_{a1})G^{cc}_{\mathbf{k}} + (\omega+\epsilon_o-\mu-\Delta \\
-Un_{a2} + n_q\omega_{1\mathbf{q}})G^{1b^+}_{\mathbf{k+q}} = 0, \\
g_{1\mathbf{kq}}(1+n_q-n_{a1})G^{cc}_{\mathbf{k}} + (\omega+\epsilon_o-\mu-\Delta \\
-Un_{a2} - n_q\omega_{1\mathbf{q}})G^{1b}_{\mathbf{k-q}} = 0, \\
-g_{2\mathbf{kq}}(n_p + n_{a2})G^{cc}_{\mathbf{k}} + (\omega+\epsilon_o-\mu+\Delta \\
-Un_{a1} + n_p\omega_{2\mathbf{q}})G^{2p^+}_{\mathbf{k-q}} = 0, \\
g_{2\mathbf{kq}}(1+n_p-n_{a2})G^{cc}_{\mathbf{k}} + (\omega+\epsilon_o-\mu+\Delta \\
-Un_{a1} - n_p\omega_{2\mathbf{q}})G^{2p}_{\mathbf{k-q}} = 0.
\end{gathered} \tag{4}$$

The M–O bond fluctuations are described by the following two operators of hole creation by oxygen and electron annihilation by a metal ion:

$$\begin{gathered}
i\frac{d}{dt}(c_i a^+_{i,1}) = (c_i a^+_{i,1})(n_{a1}(\epsilon_o-\epsilon_d-\Delta) \\
-\mu(n_c+n_{a1}) - n_{a2}(U+\epsilon_d)) \\
-n_{a2}\sum_{h1} t_{2,i,h1}(c_{i+h1}a^+_{i+h1,1}) \\
-n_{a2}\sum_{h1} t_{2,i,h1}(a^+_{i+h1,2}c_{i+h1}) \\
+n_{a2}\sum_q g_{1iq}(b^+_q + b_{-q}),
\end{gathered}$$

$$\begin{gathered}
i\frac{d}{dt}(a^+_{k,2}c_k) = (a^+_{k,2}c_k)(n_{a2}(\epsilon_o-\epsilon_d+\Delta) \\
-\mu(n_c+n_{a2}) - n_{a1}(U+\epsilon_d)) \\
+n_{a1}\sum_{h1} t_{2,k,h1}(a^+_{k+h1,2}c_{k+h1}) \\
-n_{a1}\sum_{h1} t_{2,k,h2}(c_{k+h1}, a^+_{k+h1,1}) \\
+n_{a1}\sum_q g_{2kq}(p^+_q + p_{-q}),
\end{gathered} \tag{5}$$

$$\begin{gathered}
i\frac{d}{dt}p_q = \omega_2 p_q + \sum_l g_{2l}(a_{l,2}c^+_l + a^+_{l,2}c_l), \\
i\frac{d}{dt}b_q = \omega_1 b_q + \sum_i g_{1i}(a_{i,1}c^+_i + a^+_{i,1}c_i).
\end{gathered}$$

To derive these equations, we used the law of conservation of charge $M^{+3-\delta}$–$O^{-2+\delta}$, which is related to the transfer of an electron density from oxygen to the metal cation, and neglected correlation effects between different orbitals. The parameter δ determines the covalent contribution on the ion. We write the operator of two fermions in the form

$$\tau_k = \sum_q c_{k+q}a^+_{q,1}, \quad d_k = \sum_q a^+_{q,2}c_{k+q},$$

and introduce Green's functions $G^{\tau\tau}_{\mathbf{k}} = \langle\langle\tau_{\mathbf{k}}|\tau^+_{\mathbf{k}}\rangle\rangle$, $G^{d\tau}_{\mathbf{k}} = \langle\langle d_{\mathbf{k}}|\tau^+_{\mathbf{k}}\rangle\rangle$, $G^{b\tau}_{\mathbf{k}} = \langle\langle b_{\mathbf{k}}|\tau^+_{\mathbf{k}}\rangle\rangle$, and $G^{p\tau}_{\mathbf{k}} = \langle\langle p_{\mathbf{k}}|\tau^+_{\mathbf{k}}\rangle\rangle$ for one type of bond. The corresponding set of equations is

$$\begin{gathered}
(\omega - a_{1,\tau})G^{\tau\tau}_{\mathbf{k}} + n_{a2}\varepsilon_2(\mathbf{k})G^{d\tau}_{\mathbf{k}} \\
+ g_{1\mathbf{k}}n_{a2}G^{b\tau}_{\mathbf{k}} = G^1, \\
n_{a1}\varepsilon_2(\mathbf{k})G^{\tau\tau}_{\mathbf{k}} + (\omega - a_{1,d})G^{d\tau}_{\mathbf{k}} + g_{2\mathbf{k}}n_{a1}G^{p\tau}_{\mathbf{k}} = 0, \\
g_{1\mathbf{k}}G^{\tau\tau}_{\mathbf{k}} + (\omega-\omega_1)G^{b\tau}_{\mathbf{k}} = 0, \\
-g_{2\mathbf{k}}G^{d\tau}_{\mathbf{k}} + (\omega-\omega_2)G^{p\tau}_{\mathbf{k}} = 0, \\
a_{1\tau} = n_{a1}(\epsilon_0-\epsilon_d-\Delta) - \mu(n_c+n_{a1}) \\
-n_{a2}(U+\epsilon_d) - n_{a2}\varepsilon_2(\mathbf{k}), \\
a_{1d} = n_{a2}(\epsilon_o-\epsilon_d+\Delta) - \mu(n_c+n_{a2}) \\
-n_{a1}(U+\epsilon_d) + n_{a1}\varepsilon_2(\mathbf{k}), \\
\varepsilon_2(\mathbf{k}) = -2t_2(\cos k_x + \cos k_y + \cos k_z).
\end{gathered} \tag{6}$$

The set of equations for Green's functions for another type of bond,

$$\begin{gathered}
G^{dd}_{\mathbf{k}} = \langle\langle d_{\mathbf{k}}|d^+_{\mathbf{k}}\rangle\rangle, \quad G^{\tau d}_{\mathbf{k}} = \langle\langle\tau_{\mathbf{k}}|d^+_{\mathbf{k}}\rangle\rangle, \\
G^{bd}_{\mathbf{k}} = \langle\langle b_{\mathbf{k}}|d^+_{\mathbf{k}}\rangle\rangle, \quad G^{pd}_{\mathbf{k}} = \langle\langle p_{\mathbf{k}}|d^+_{\mathbf{k}}\rangle\rangle,
\end{gathered}$$

has the form

$$\begin{gathered}
(\omega - a_{1,d})G^{dd}_{\mathbf{k}} + n_{a1}\varepsilon_2(\mathbf{k})G^{\tau d}_{\mathbf{k}} + g_{2\mathbf{k}}n_{a1}G^{pq}_{\mathbf{k}} = G^2, \\
n_{a2}\varepsilon_2(\mathbf{k})G^{dd}_{\mathbf{k}} + (\omega - a_{1,\tau})G^{\tau d}_{\mathbf{k}} + g_{1\mathbf{k}}n_{a2}G^{b\tau}_{\mathbf{k}} = 0, \\
(-\omega+\omega_2)G^{pq}_{\mathbf{k}} + g_{2\mathbf{k}}G^{dd}_{\mathbf{k}} = 0, \\
(-\omega+\omega_1)G^{b\tau}_{\mathbf{k}} - g_{1\mathbf{k}}G^{\tau d}_{\mathbf{k}} = 0.
\end{gathered} \tag{7}$$

The chemical potential is computed by a self-consistent procedure via the numerical solution of the set of the three equations

$$n_c = \frac{1}{N}\sum_{\mathbf{k},\mathbf{q}}\int d\omega f(\omega)\frac{1}{\pi}\mathrm{Im}G^{cc}_{\mathbf{k},\mathbf{q}},$$

$$n_{a1} = \frac{1}{N}\sum_{\mathbf{k},\mathbf{q}}\int d\omega f(\omega)\frac{1}{\pi}\mathrm{Im}G^{11}_{\mathbf{k},\mathbf{q}}, \quad (8)$$

$$n_{a2} = \frac{1}{N}\sum_{\mathbf{k},\mathbf{q}}\int d\omega f(\omega)\frac{1}{\pi}\mathrm{Im}G^{22}_{\mathbf{k},\mathbf{q}},$$

where $f(\omega) = (\exp(\omega/T) + 1)^{-1}$. From summation over momenta, we can pass to integration by making allowance for the initial density of states or can directly calculate the sum over the electron and phonon momenta in the first Brillouin zone at a step $\Delta k = 0.2$ for 10^9 points, which is impossible for modern computers. To bypass this problem, we assume that the optical modes and the exciton (electron + hole)–phonon coupling function are independent of the momentum q. This formulation is equivalent to the consideration of interaction with long-wavelength optical vibration modes.

The dynamic conductivity σ is computed by the Kubo–Greenwood formula [19]

$$\sigma = \sum_{\mathbf{k}}\int d\omega\left(-\frac{\partial f(\omega)}{\partial\omega}\right)\left(\frac{1}{\pi}\right)^2$$

$$\times(\mathrm{Im}G^{cc}_{\mathbf{k}} + \mathrm{Im}G^{11}_{\mathbf{k}} + \mathrm{Im}G^{22}_{\mathbf{k}})^2,$$

$$L_{12} = -Te\sum_{\mathbf{k}}\int d\omega\left(-\frac{\partial f(\omega)}{\partial\omega}\right)\omega(\mathbf{k})\left(\frac{1}{\pi}\right)^2$$

$$\times\left(\sum_{\alpha}\mathrm{Im}G^{\alpha\alpha}_{\mathbf{k}}\right)^2, \quad (9)$$

$$L_{22} = T\sum_{\mathbf{k}}\int d\omega\left(-\frac{\partial f(\omega)}{\partial\omega}\right)\omega^2(\mathbf{k})\left(\frac{1}{\pi}\right)^2$$

$$\times\left(\sum_{\alpha}\mathrm{Im}G^{\alpha\alpha}_{\mathbf{k}}\right)^2,$$

$$S = \frac{L_{12}}{T\sigma}, \quad k = \left(\frac{-L^2_{12}}{L_{11}} + L_{22}\right)\frac{1}{T},$$

where the summation over α is taken for both the one-particle Green's functions of electrons and holes and the two-particle electron + hole Green's functions determined from Eqs. (6) and (7).

3. DISCUSSION OF RESULTS

Actually, the orthorhombic anisotropy in Eqs. (1) reflects the interaction of the oxygen pseudospin orbital moments $\tau^z = a_1^+ a_1 - a_2^+ a_2$ with the field created by rare-earth ions and splits the band into two subbands, which begin to diverge as the orthorhombic anisotropy parameter increases. Two narrow polaron minisubbands form near the gap, and their positions change as a function of the electron–phonon interaction constant. One of them is located under the valence band top and results from the interaction of electrons with the bending vibration mode. The other level lies near the conduction band bottom and is caused by the interaction of electrons with the stretching modes of the octahedron. The electron states localized on the $3d$ metal ions have high energies and are represented by a number of lines in the energy range $\omega/t = 10$–15 in Figs. 1a and 1b. The typical behavior of the density of states for various electron–phonon interaction parameters is illustrated in Fig. 1. For small parameters ($g_1 \ll 1$, $g_2 \ll 1$), the polaron minisubbands contract and form narrow lines, similar to impurity states in semiconductors. Their relative position with respect to the chemical potential specifies the temperature behavior of resistivity.

For the phonon frequencies characteristic of a perovskite structure ($\omega_1/t = 0.25$–0.3, $\omega_2/t = 0.45$–0.5) and the orthorhombic distortion parameter corresponding to the Jahn–Teller lattice distortions ($\Delta/t = 1$–2), we can obtain various dependences for the temperature behavior of resistivity, which are determined by the electron–phonon interaction parameters and the orthorhombic distortion of the crystal field. The decrease in the gap width with increasing temperature shifts the valence band top with respect to the chemical potential, and, at a certain critical temperature, the chemical potential moves into the band, which causes a sharp decrease in the resistivity. Figure 2a shows two $\rho(T)$ dependences for two orthorhombic anisotropy parameters ($\Delta/t = 1.5$, 1.25) at an oxygen band occupation number $n_{a1} + n_{a2} = 0.2$. For $\Delta/t = 1$, the chemical potential is in the lower band. At low temperatures, a minimum is observed in the temperature behavior of resistivity at a certain temperature T_1; this minimum is related to reaching the maximum amplitude of the transition between polaron states, since the transition intensity is proportional to $g_1 g_2$ (Fig. 2a).

An increase in the interaction of the bending vibration mode with electrons causes a deviation from the linear dependence of $\ln(\rho/T)$ on $1/T$ at a temperature $T_1 < T_2$, which was detected in the $RMnO_3$ family ($T_1 = 350$–500 K, $T_2 = 750$–900 K) and in the $RNiO_3$ family ($T_1 = 100$–140 K, $T_2 = 400$–500 K) [10]. According to our calculations, the chemical potential of the $RMnO_3$ (R = La, Pr, Nd) manganites is inside the energy gap between the oxygen subbands. Upon heating, the gap narrows and the chemical potential falls in the lower oxygen band. As a result, the resistivity drops at a temperature T_2, which increases with the orthorhombic

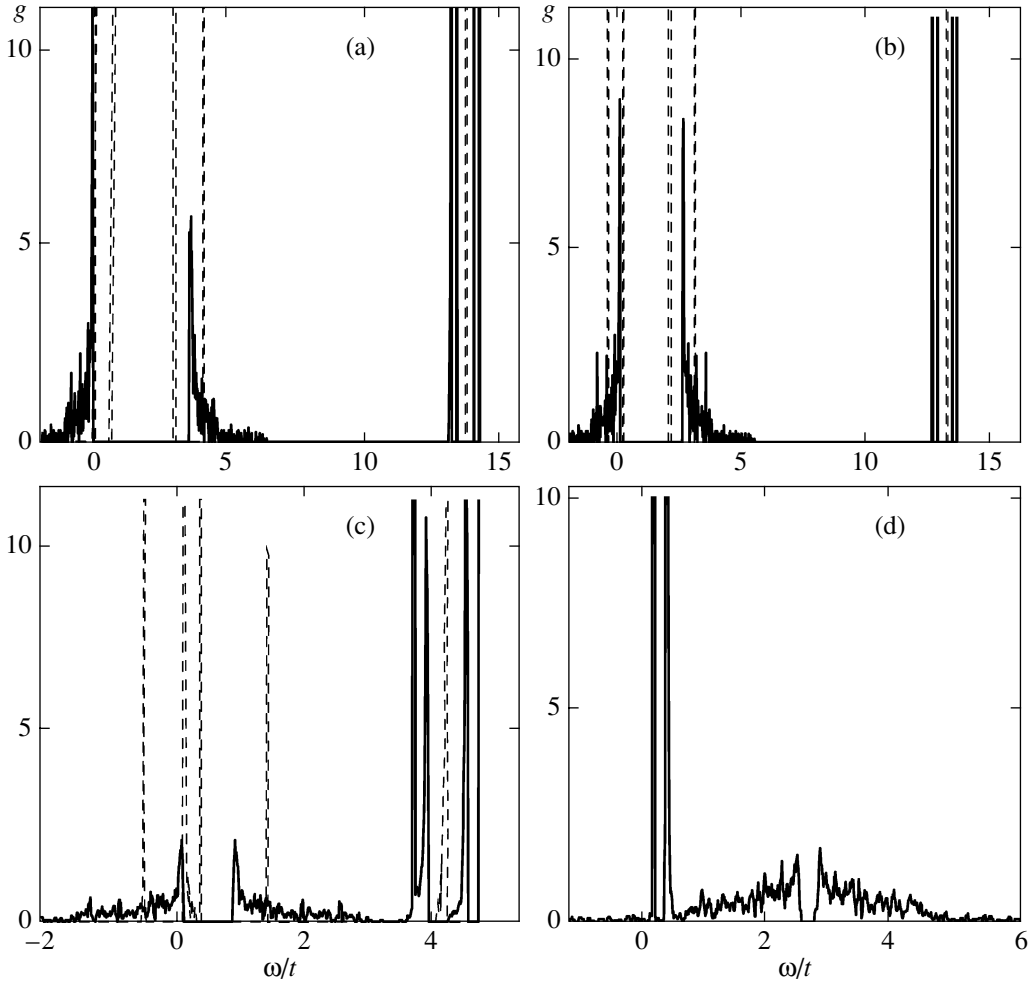

Fig. 1. Density of states for one-particle electron excitations at the following parameters: (a) $\Delta = 1.5$, $U = 3$, $\omega_1 = 0.25$, $\omega_2 = 0.4$, $g_1 = 0.02$, $g_2 = 0.3$, $n_c = 0.2$, $\epsilon_o - \epsilon_d = 15$, and $T = 0.02$; (b) the same and $T = 0.6$; and (c) $\Delta = 1.0$, $g_1 = 0.6$, $g_2 = 0.05$, $n_c = 0.32$, $\epsilon_o - \epsilon_d = 5$, and $T = 0.02$. The density of states for two-particle (electron + hole) excitations at (d) $\Delta = 1.5$, $U = 3$, $\omega_1 = 0.25$, $\omega_2 = 0.4$, $g_1 = 0.02$, $g_2 = 0.3$, $n_c = 0.2$, $\epsilon_o - \epsilon_d = 15$, and $T = 0.02$.

anisotropy field. This behavior correlates qualitatively with the experimental dependence of T_{JT} on the Mn–O–Mn bond angle shown in Fig. 2 [2]. The dependence of the amplitude of oxygen-atom thermal vibrations directed normal to the Mn–O bond ($u(T) - u(T_2)$) is qualitatively similar to the $\rho(T)$ dependence. At $T < T_1$, the oxygen-atom vibrations directed normal to this bond weaken sharply, whereas the vibration amplitude along this bond remains virtually unchanged as the temperature decreases to $T = 300$ K [4].

When comparing the calculated $\rho(T)/\rho(T_{JT})$ temperature dependence with the experimental data for $LaMnO_3$, we estimate the hopping integral at $t = 0.18$ eV and obtain good agreement between the frequencies used for our calculations ($\omega_1 = 0.045$ eV, $\omega_2 = 0.076$ eV) and the experimental data in [17] ($\omega_{\text{bending}} \approx 0.044$ eV, $\omega_{\text{stretching}} \approx 0.074$ eV). The electron–phonon interaction parameters ($g_1 = 0.02$, $g_2 = 0.3$) fall in the range whose lower boundary ($\hat{g}_l \sim 0.04$ eV) was determined when calculating orbital excitations (orbitrons) [20], and upper boundary ($\hat{g}_{up} \sim 0.2$ eV) was found in the model of interaction of electrons with phonons and localized spins [21]. The static Jahn–Teller energy ($E_{JT} = 0.25$ eV [21]) agrees well with the orthorhombic distortion parameter ($\Delta \approx 0.27$ eV) used in our calculations. During the transition through the orbital ordering temperature, the magnetic moment in $LaMnO_3$ changes ($\delta\mu_{\text{eff}} = 0.11\mu_B$), which is related to the formation of the charge disproportionation Mn^{+3}, $Mn^{+3-\delta}$ [5], which is consistent with our parameters used in the calculations ($\delta = n_{a1} + n_{a2} = 0.2$).

The thermoelectric power shown in Fig. 3 also decreases near the critical temperature, although this change differs by several times from the experimental value. This is likely to be caused by the neglected inter-

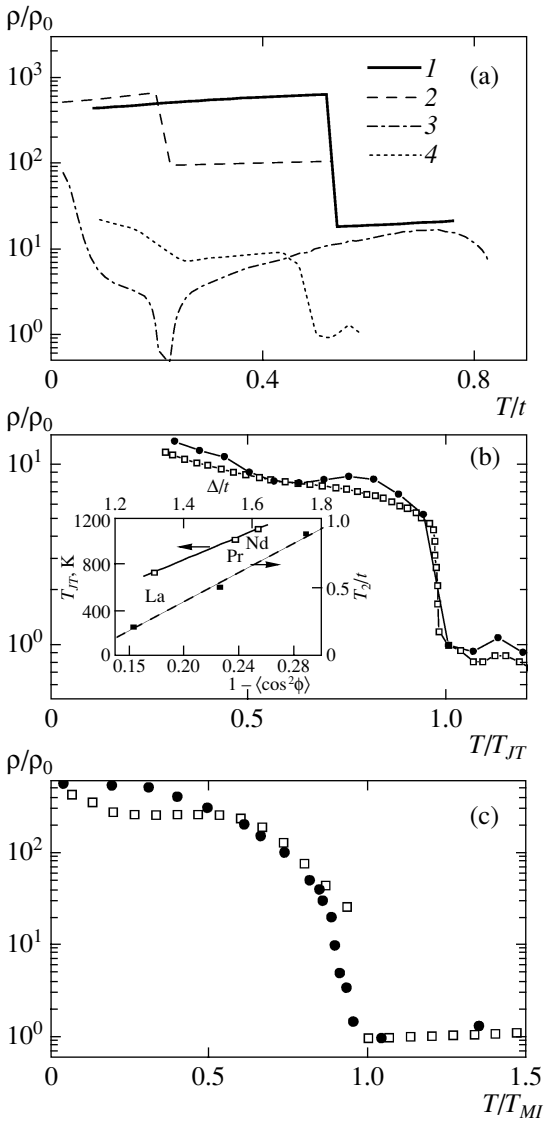

Fig. 2. (a) Temperature dependence of the resistivity $\rho(T)/\rho_0$ normalized by the constant that determines the dimension of resistivity at the following parameters: (*1*) $\epsilon_o - \epsilon_d = 15$, $U = 3$, $\omega_1 = 0.25$, $\omega_2 = 0.4$, $n_c = 0.2$, $g_1 = 0.02$, $g_2 = 0.02$, and $\Delta = 1.5$; (*2*) $g_1 = 0.03$, $g_2 = 0.3$, and $\Delta = 1.25$; (*3*) $g_1 = 0.03$, $g_2 = 0.3$, and $\Delta = 1.5$; and (*4*) $g_1 = 0.5$, $g_2 = 0.5$, and $\Delta = 1.5$. (b): (○) The resistivity normalized by the Jahn–Teller temperature in $LaMnO_3$ $\rho(T)/\rho_0(T_{JT})$ [2] and (●) our calculations at parameters $g_1 = 0.03$, $g_2 = 0.3$, and $\Delta = 1.5$. The inset shows (●) the structural transition temperature T_{JT} vs. the Mn–O–Mn bond angle $1 - \cos^2\phi$ [2] and the temperature T_2 at which a resistivity jump occurs vs. the orthorhombic anisotropy Δ. (c): (□) The resistivity normalized by the metal–insulator transition temperature in $PrNiO_3$ $\rho(T)/\rho_0(T_{MI})$ [10] and (●) our calculations at parameters $\epsilon_o - \epsilon_d = 5$, $U = 3$, $\omega_1 = 0.25$, $\omega_2 = 0.4$, $n_c = 0.32$, $g_1 = 0.6$, $g_2 = 0.03$, and $\Delta = 1.0$.

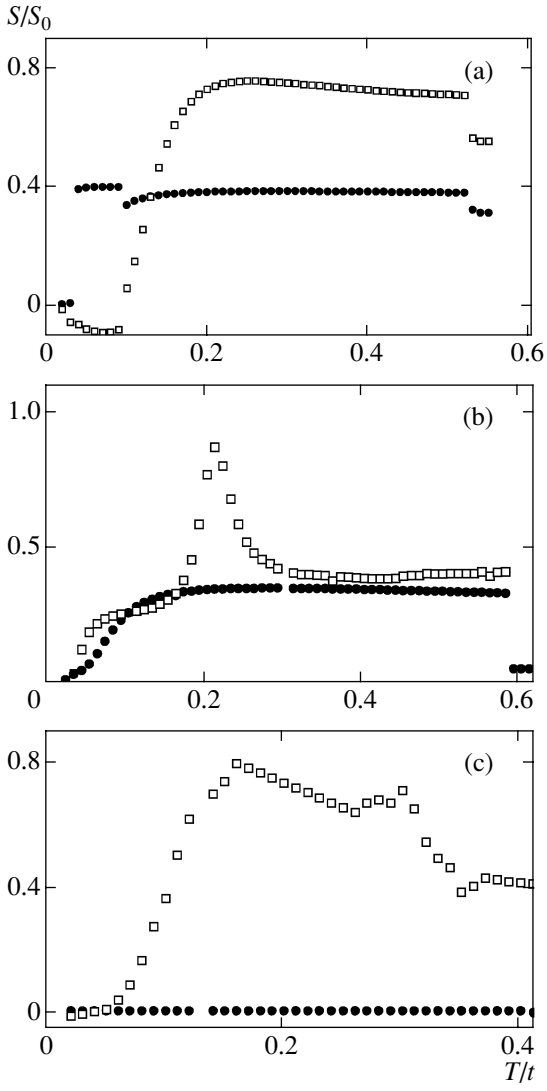

Fig. 3. Thermopower coefficient normalized by the constant S_0 that determines the dimension of thermopower that is caused by (□) one-particle excitation and (●) two-particle excitations at (a) $\Delta = 1.5$, $g_1 = 0.03$, and $g_2 = 0.3$; (b) $g_1 = 0.5$ and $g_2 = 0.5$; and (c) $\epsilon_o - \epsilon_d = 5$, $U = 3$, $n_c = 0.32$, $g_1 = 0.6$, $g_2 = 0.03$, and $\Delta = 1.0$.

action of the electron and orbital subsystems with acoustic vibration modes. In manganites in the temperature range 150–200 K, the thermoelectric-power mechanism can change from a one-polaron to a two-particle exciton mechanism. An increase in the electron–phonon interaction constant causes anomalies in the thermal conductivity (Fig. 4) and the thermoelectric power in the temperature range corresponding to the minimum resistivity. The polaron mechanism dominates over the exciton one. The density of two-particle excitations is maximal in the range of bending and stretching modes of the octahedron (Fig. 1d).

According to photoemission spectra, the chemical potential in nickelates is located in the upper part of the band. In our model, the chemical potential falls in the lower oxygen band, which is split by an orthorhombic anisotropy $\Delta/t = 1$. At certain temperatures, electron

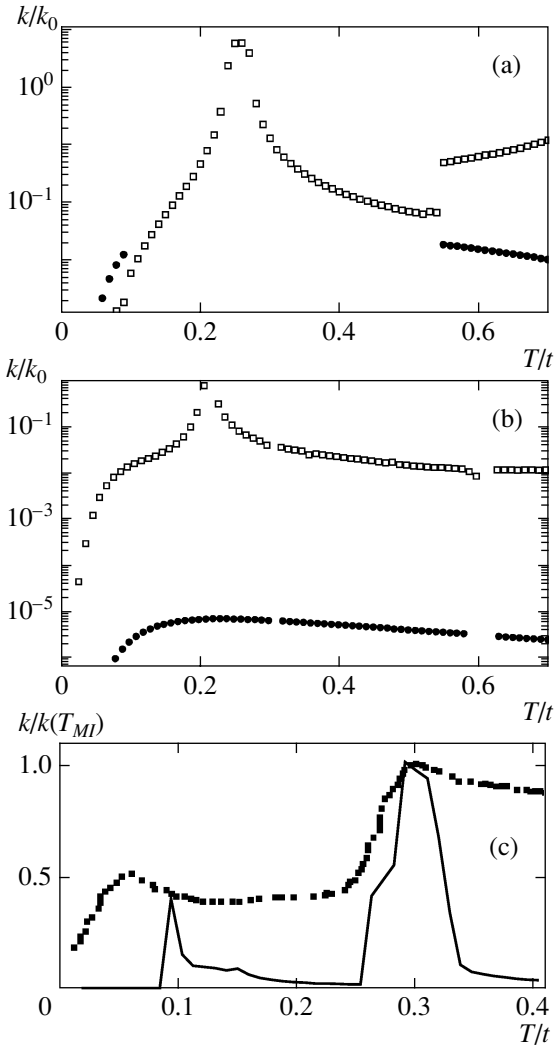

Fig. 4. Thermal conductivity normalized by the constant k_0 that determines the dimension of thermal conductivity due to (□) one-particle excitation and (●) two-particle excitations: (a) $\Delta = 1.5$, $g_1 = 0.03$, $g_2 = 0.3$; (b) $g_1 = 0.5$, $g_2 = 0.5$; (c) (curve) $\epsilon_o - \epsilon_d = 5$, $U = 3$, $n_c = 0.32$, $g_1 = 0.6$, $g_2 = 0.03$, and $\Delta = 1.0$; (●) $PrNiO_3$ [10].

transitions from the lower subband to the polaron levels inside the gap (Fig. 1c) cause a sharp decrease in the resistivity (Fig. 2c) and two maxima in the thermal conductivity (Fig. 4c). The temperatures of the corresponding anomalies in the behavior of the transport properties depend on the electron–phonon interaction and the vibration-mode frequency of the octahedron. The two-particle (exciton) contribution to the thermal conductivity and thermoelectric power is several orders of magnitude smaller than the contribution of the polaron mechanism of the transport properties in nickelates.

The temperature T_1 corresponding to the maximum in the temperature behavior of the thermal conductivity (Fig. 4c; for $PrNiO_3$, $T_1 \approx 30$ K) and the MI transition temperature ($T_2 = 130$ K [10]) are used to estimate the hopping integrals ($t \sim 0.1$ eV) and the orthorhombic distortion parameter ($\Delta \sim 0.1$ eV) at $g_1 = 0.6$ and $g_2 = 0.03$. The change in the resistivity by two orders of magnitude in the range of the MI transition in $RNiO_3$ (R = Pr, Nd) is well described in terms of our model. This change in the resistivity is caused by the predominant interaction of electrons with the bending modes of the octahedron. The optical conductivity in the infrared region in nickelates is explained by a strong electron–phonon interaction with the following three vibration modes: $\omega_1 \approx 0.024$ eV, $\omega_2 \approx 0.049$ eV, and $\omega_3 \approx 0.062$ eV [22], where ω_2 and ω_3 are the antisymmetric and symmetric stretching modes of the octahedron, respectively. The vibration frequencies used in our calculations ($\omega_1 = 0.025$ eV, $\omega_2 = 0.05$ eV) virtually coincide with the experimental frequencies.

The fact that the electron–phonon coupling is strong is supported by a colossal isotopic effect at T_{MI} [10] and the maximum of the Ni–O bond length dispersion near the transition temperature T_{MI}. For example, octahedron distortions become maximal near the transition temperature T_{MI} and decrease with decreasing temperature. The distortion parameter in $SmNiO_3$ ($\Delta_d = 1/6\sum_{1,6}[(d_n - \langle d\rangle)/\langle d\rangle^2]^2 \sim 1.6 \times 10^{-5}$ [23]) is two orders of magnitude smaller than that in $LaMnO_3$ ($\Delta_d \sim 3.3 \times 10^{-3}$ [23]). In nickelates, the $Me^{+3-\delta}$–$O^{-2+\delta}$ covalent bond is stronger than in manganites. For example, according to various estimates found from the resonance x-ray scattering spectra recorded with a nickel K line, $\delta = 0.42 \pm 0.04e$ in $NdNiO_3$ [24] and increases with decreasing ionic radius of the rare-earth element; for Ho and Y, it is $\delta \approx 0.6e$ [25]. The weight of the $3d^8L$ electronic states found from photoemission spectra ranges from 0.3 to 0.56 [26]. The conductivity calculations of nickelates were performed at the parameters that are consistent with the experimental data (e.g., $\delta = n_{a1} + n_{a2} = 0.32$).

4. CONCLUSIONS

We calculated the transport properties of the oxides of 3*d* metals by making allowance for the transport of one electron and two electrons at metal and oxygen ions, respectively, for a perovskite-like structure with an orthorhombic anisotropy, which results in a gap in the spectrum of electron excitations.

The formation of polaron levels, which are related to the bending and stretching modes of the octahedron, inside the gap causes sharp changes in the resistivity and maxima in the temperature dependences of the thermal conductivity and thermoelectric power. For manganites, this formation corresponds to the temperature range 300–400 K, and, at temperatures below 150 K, the thermoelectric power and thermal conductivity are caused by the two-particle excitation of a neutral quasiparticle consisting of an electron and a hole. In nickelates, the metal–insulator transition is induced by

polaron pinning by the stretching mode of the octahedron, and the low-temperature maximum of the thermal conductivity is related to electron scattering by the bending mode of the octahedron.

REFERENCES

1. P. M. Woodward, D. E. Cox, E. Moshopoulou, et al., Phys. Rev. B **62**, 844 (2000).
2. J. S. Zhou and J. B. Goodenough, Phys. Rev. B **68**, 144406 (2003).
3. K. Tobe, T. Kimura, Y. Okimmoto, and Y. Tokura, Phys. Rev. B **64**, 184421 (2001).
4. X. Qiu, Th. Proffen, J. F. Mitchell, and S. J. L. Billinge, Phys. Rev. Lett. **94**, 177203 (2005).
5. J. S. Zhou and J. B. Goodenough, Phys. Rev. B **60**, R15002 (1999).
6. J. Rodriguez-Carvajal, M. Hennion, F. Moussa, et al., Phys. Rev. B **57**, 3189 (1998).
7. T. Mizokawa, A. Fujimori, H. Namatame, et al., Phys. Rev. B **49**, 7193 (1994).
8. C. Piamonteze, H. C. N. Tolentino, A. Y. Ramos, et al., Phys. Rev. B **71**, 012104 (2005).
9. I. Vobomik, L. Perfetti, M. Zacchigna, et al., Phys. Rev. B **60**, R8426 (1999).
10. J. S. Zhou, J. B. Goodenough, and B. Dabrowski, Phys. Rev. B **67**, 020404(R) (2003).
11. P. Lunkenheimer, T. Rudolf, J. Hemberger, et al., Phys. Rev. B **68**, 245108 (2003).
12. J. Hemberger, H.-A. Krug von Nidda, V. Fritsch, et al., Phys. Rev. Lett. **91**, 066403 (2003).
13. M. C. Sanchez, G. Subias, J. Garcia, and J. Blasco, Phys. Rev. Lett. **90**, 045503 (2003).
14. D. D. Sarma, O. Rader, T. Kachel, et al., Phys. Rev. B **49**, 14238 (1994).
15. J. B. Torrance, P. Lacorre, A. I. Nazzal, et al., Phys. Rev. B **45**, 8209 (1992).
16. J. C. Slater and G. F. Koster, Phys. Rev. **94**, 1498 (1956).
17. Ch. Hartinger, F. Mayr, A. Loidl, and T. Kopp, Phys. Rev. B **70**, 134415 (2004).
18. S. Jandl, A. A. Mukhin, V. Yu. Ivanov, et al., Phys. Rev. B **72**, 024423 (2005).
19. K. Nagai, T. Momoi, and K. Kubo, J. Phys. Soc. Jpn. **69**, 1837 (2000).
20. J. van den Brink, Phys. Rev. Lett. **87**, 217202 (2001).
21. D. S. Dessau and Z. X. Shen, in *Colossal Magnetoresistance Oxides*, Ed. by Y. Tokura (Gordon and Breach, New York, 1999), Chap. 5.
22. M. A. Mroginski, N. Massa, H. Salva, et al., Phys. Rev. B **60**, 5304 (1999).
23. J. Rodriguez-Carvajal, S. Rosenkranz, M. Medarde, et al., Phys. Rev. B **57**, 456 (1998).
24. U. Staub, G. I. Meijer, F. Fauth, et al., Phys. Rev. Lett. **88**, 126402 (2002).
25. J. A. Alonso, M. J. Martinez-Lope, M. T. Casais, et al., Phys. Rev. B **61**, 1756 (2000).
26. T. Mizokawa, A. Fujimori, T. Arima, et al., Phys. Rev. B **52**, 13865 (1995).

Translated by K. Shakhlevich